



# Catalytic transfer hydrogenation of butyl levulinate to $\gamma$ -valerolactone over zirconium phosphates with adjustable Lewis and Brønsted acid sites



Fukun Li, Liam John France, Zhenping Cai, Yingwen Li, Sijie Liu, Hongming Lou, Jinxing Long\*, Xuehui Li\*

School of Chemistry and Chemical Engineering, Pulp & Paper Engineering State Key Laboratory of China, South China University of Technology, Guangzhou, Guangdong, 510640, China

## ARTICLE INFO

### Article history:

Received 5 January 2017

Received in revised form 25 March 2017

Accepted 3 May 2017

Available online 3 May 2017

### Keywords:

$\gamma$ -Valerolactone

Butyl levulinate

Zirconium phosphate

Transfer hydrogenation

Catalytic mechanism

## ABSTRACT

The efficient production of  $\gamma$ -valerolactone (GVL) from renewable resources is attracting increasing attention in view of its wide application in fuel and synthetic chemistry. In this study, a series of novel and efficient zirconium phosphate catalysts were developed for the transfer hydrogenation of levulinic esters to GVL using isopropanol as the hydrogen donor. Experimental results show that 98.1% butyl levulinate conversion and 95.7% GVL yield can be achieved with ZrPO-1.00 at 483 K after 2.0 h. Intensive characterization of the synthesized catalysts using  $N_2$  adsorption-desorption, FT-IR, ICP-AES, XPS,  $NH_3$ -TPD, Py-FTIR and XRD demonstrates that the physicochemical properties, particularly hydrophobicity, Lewis to Brønsted acid site ratio and Lewis acid site strength were subtly tuned via adjustment of the molar proportion of phosphorus to zirconium, which is responsible for excellent transfer hydrogenation activity. Furthermore, this optimized catalyst exhibits high stability and recyclability for at least ten reaction cycles. In addition, a plausible reaction pathway and catalytic mechanism are proposed.

© 2017 Elsevier B.V. All rights reserved.

## 1. Introduction

Diminishing worldwide fossil resources and increasingly serious environmental issues, such as airborne pollution and climate change, urge people to explore and utilize sustainable alternatives. Biomass is a unique carbon-containing renewable global resource, so the efficient catalytic conversion of this natural material to platform chemicals and bio-fuels is a promising approach to realize a carbon cycle [1,2]. Various bio-chemicals, for example, 5-hydroxymethylfurfural, furfural, lactic acid, etc., have been obtained from lignocellulosic biomass *via* a number of procedures [3]. As a versatile bio-chemical (Scheme S1),  $\gamma$ -valerolactone (GVL) can be directly used as a high quality fuel additive due to its  $\Delta H_{c,liq}$  value of  $-2.65\text{ MJ mol}^{-1}$  ( $-1.37$  and  $-3.37\text{ MJ mol}^{-1}$  for ethanol and methyl *tert*-butyl ether respectively) [4], is an ideal solvent for organic synthesis and biomass pre-treatment [5,6]. At the same time, it is an eco-friendly starting material for the preparation of a series of important fine chemicals (e.g., 1, 4-pentanediol, pentanoic acid, 2-methyl tetrahydrofuran, etc.) [7]. Generally, GVL can be

obtained directly from the depolymerization of renewable biomass *via* various domino reaction pathways. For instance, glucose can be generated by the hydrolysis of cellulose, which is then isomerized to fructose, 5-hydroxymethylfurfural is obtained by dehydration of fructose and converted to levulinic acid (LA) or its ester *via* rehydration [8,9]. GVL is finally produced by lactonization of alkyl 4-hydroxypentanoate, which is obtained through hydrogenation of LA or its ester [10]. Usually hydrogenation is the crucial step in all the above processes, due to the need of special catalysts to meet the requirements of different hydrogen sources. Therefore, numerous efforts have been made to develop novel and efficient catalytic hydrogenation systems for this reaction [10].

There are two types of hydrogenation technology for GVL formation, direct and transfer hydrogenation. The former is usually conducted over a series of noble metal catalysts (such as Ru, Au-Pd and Pd) in the presence of molecular hydrogen ( $>30$  bar) [11,12], but this is obviously limited by the high cost of the catalyst, excessive hydrogenation of substrate, high pressure hydrogen, etc. In contrast, transfer hydrogenation using formic acid or alcohols as hydrogen donors is more attractive and safe due to the absence of molecular hydrogen [13,14]. Noble metal catalysts (such as Au, Pt, Pd and Ru) are often utilized as they have good catalytic activity [15,16]. However, the high cost of these metals makes this strategy

\* Corresponding authors.

E-mail addresses: [cejxlong@scut.edu.cn](mailto:cejxlong@scut.edu.cn) (J. Long), [cexhli@scut.edu.cn](mailto:cexhli@scut.edu.cn) (X. Li).

an unattractive proposition. As such, a series of non-noble metal catalysts (such as Raney Ni,  $\text{Fe}_3(\text{CO})_{12}$ , CuO and Zr-based materials) have been developed [17–20]. Among which, Raney Ni and CuO based on metal hydride and *in-situ*  $\text{H}_2$  formation routes respectively. But, they are restricted partly by the stability of the catalyst, for example, Raney Ni is very sensitive to air and CuO is readily reduced to  $\text{Cu}_2\text{O}$  or metallic Cu. Compared to these catalytic systems, Zr-containing materials based on Meerwein-Ponndorf-Verly (MPV) reduction have attracted significant attention due to their high chemical stability and outstanding catalytic activities. For example,  $\text{ZrO}_2$  and  $\text{Zr}(\text{OH})_4$  were used previously as solid bases to convert levulinic esters to GVL [20,21]. Zr-Beta, a typical Lewis acid catalyst, was also employed, its activity is mainly influenced by the hydrophobicity of the catalyst and the addition of strong Brønsted acid sites [22,23]. Recently, Zr-HBA and Zr-Phy were utilized for the conversion of levulinic esters to GVL in isopropanol, where excellent GVL yield could be obtained by modification of the acid and base sites of the catalyst [24,25]. Similarly,  $\text{ZrOCl}_2 \cdot 8\text{H}_2\text{O}$ , Zr-CA, Zr-MOF, Ni-Zr and Al-Zr mixed oxides had been applied in this reaction [26–30]. However, the synergistic effect of both acidic sites and their catalytic mechanism for GVL production needs to be further investigated.

It has been previously demonstrated that Lewis acid sites are responsible for converting LA and its esters to alkyl 4-hydroxypentanoate [23,31], which is then converted to GVL in the presence of Brønsted acid sites [32,33], but most current studies ignore the synergistic effect between the two different acid sites. Zirconium phosphate, another important and environmentally benign material, has found application in the biomass refinery and features both adjustable Brønsted and Lewis acid sites [34–40]. To the best of our knowledge, little information regarding its performance for transfer hydrogenation of carbonyl compounds has been studied. In this report, the production of GVL by transfer hydrogenation of LA and its esters is investigated using zirconium phosphate as the catalyst and isopropanol as the hydrogen donor. The influence of varying the ratio between Lewis and Brønsted acid sites and their catalytic mechanism for GVL production were discussed by examination of the relationships between catalyst composition, physiochemical properties and catalytic activity. In addition, the effect of reaction parameters and catalyst deactivation were discussed, and a plausible reaction pathway was proposed.

## 2. Experimental

### 2.1. Materials

Levulinic acid (99%), isopropanol (99%), methyl levulinate (97%) and  $\gamma$ -valerolactone (98%) were purchased from J&K Scientific Ltd (Beijing, China). Ethyl levulinate (98%), butyl levulinate (98%) and naphthalene (98%) were purchased from TCI (Shanghai, China). Other reagents were purchased from Guanghua Chemical Factory Co. Ltd (Guangdong, China). All reagents were of analytical grade and used without further purification.

Propyl levulinate and isopropyl levulinate were synthesized by esterification of LA with the corresponding alcohol catalyzed with concentrated HCl solution and purified through distillation. Gas chromatography-flame ionization detection (GC-FID) analysis showed that their purities were greater than 99%.

### 2.2. Catalyst preparation

The zirconium phosphate catalysts ( $\text{ZrPO-X}$ , where X stands for the theoretical molar ratio of phosphorus to zirconium, namely  $\text{P}/\text{Zr}$ ) were prepared according to the reported literature [34]. In a typical  $\text{ZrPO-1.00}$  preparation, a solution of  $\text{NH}_4\text{H}_2\text{PO}_4$  (1.0 mol L<sup>-1</sup>,

70 mL) was added rapidly to a solution of  $\text{ZrOCl}_2 \cdot 8\text{H}_2\text{O}$  (0.5 mol L<sup>-1</sup>, 140 mL) under vigorous stirring at room temperature. The obtained white precipitate was filtered, washed with deionized water (200 mL  $\times$  3), dried at 373 K for 24 h, ground to a powder and calcined at 673 K for 4.0 h to obtain the  $\text{ZrPO-1.00}$  sample. Other catalysts were prepared following the same procedure with varying  $\text{NH}_4\text{H}_2\text{PO}_4$  concentrations.

### 2.3. Catalyst characterization

$\text{N}_2$  adsorption-desorption isotherms were collected on a Micromeritics ASAP 2020 micropore size analyzer at 77 K. Samples were degassed at 473 K for 12 h under vacuum prior to measurement. The surface area ( $S_{\text{BET}}$ ) was calculated from the linear portion of the plot according to the Brunauer–Emmett–Teller (BET) method. The pore size distribution was calculated using the adsorption branch of the nitrogen adsorption–desorption isotherm by the Barrett–Joyner–Halenda (BJH) method. The single-point pore volume ( $V_{\text{pore}}$ ) was calculated from the adsorption isotherm at a relative pressure of 0.99. Average pore size ( $D_{\text{mean}}$ ) was calculated from the adsorption average pore diameter (4V/A by BET).  $\text{H}_2\text{O}$  vapor adsorption isotherms were measured on a 3H-2000PW apparatus at 298 K. Samples were degassed at 473 K for 12 h under vacuum prior to measurement.  $X_{0.15}$ , a good metric to evaluate surface hydrophobicity, was calculated by the ratio between volumetric  $\text{H}_2\text{O}$  uptake to that of nitrogen at  $P/P_0 = 0.15$  [41–43].

X-ray diffraction (XRD) patterns of the samples were recorded on a Rigaku D/MAX-3A Auto X-ray diffractometer with  $\text{Cu K}\alpha$  radiation ( $\lambda = 0.15418 \text{ nm}$ ) operated at 40 kV and 40 mA over a  $2\theta$  range of 10–80° with a 0.05° step size and a counting time of 1 s per point. X-ray photoelectron spectroscopy (XPS) experiments were performed on a Thermo ESCALAB 250Xi with a hemispherical detector operating at constant pass energy (100.0 eV) and an X-ray source at 150 W and  $\text{Al K}\alpha$  radiation (1486.6 eV). The carbon content of the spent catalyst was determined on a Vario EL III elemental analyzer, samples were dried at 373 K for 12 h under vacuum prior to analysis. Thermal analysis was performed on a NETZSCH STA 449C. Before analysis, all samples were dried at 333 K for 12 h under vacuum, then, approximately 4 mg of sample was heated from 308 to 1073 K at a rate of 10 K min<sup>-1</sup> with an air flow rate of 40 mL min<sup>-1</sup>.

The contents of P and Zr in the bulk samples were determined by inductively coupled plasma atomic emission spectroscopy (ICP-AES) on a Prodigy High Dispersion ICP apparatus (Prodigy, Leeman Teledyne). Prior to measurement, the sample was dried at 333 K for 12 h under vacuum, then, 60 mg of sample was dissolved in concentrated hydrofluoric acid (40 wt% in water). The resulting solution was diluted with distilled water until the concentration of the measured ion was in the range of 1–9 mg L<sup>-1</sup>.

Sample acidity was studied with temperature programmed desorption of  $\text{NH}_3$  ( $\text{NH}_3$ -TPD) using a Micromeritics AutoChem II 2920 chemisorption analyzer coupled with a thermal conductivity detector. Approximately 100 mg of sample was degassed at 673 K for 1.0 h and cooled to 373 K under 20 mL min<sup>-1</sup> He.  $\text{NH}_3$  was adsorbed for 0.5 h, after which He (20 mL min<sup>-1</sup>) was introduced to purge the system and remove physically adsorbed  $\text{NH}_3$  for 2.0 h. The resulting sample was heated to 1073 K at a rate of 10 K min<sup>-1</sup> in a He flow of 20 mL min<sup>-1</sup>.

Fourier transform infrared (FT-IR) spectra were recorded between 400 to 4000 cm<sup>-1</sup> on a Bruker VERTEX 33 spectrometer using KBr pellets. Before the test, the sample was dried at 333 K for 12 h under vacuum. The Brønsted and Lewis acid sites of the sample were determined by FT-IR spectra with pyridine as the probe molecule (Py-FTIR) using a Bruker Tensor 27 spectrometer at 4 cm<sup>-1</sup> resolution. Prior to analysis, approximately 25 mg of sample was pressed into a 13 mm self-supported wafer and activated in the

IR cell at 673 K for 4.0 h at 10<sup>-3</sup> Pa. Following which, it was cooled to room temperature, the sample was exposed to pyridine vapor under vacuum for 0.5 h followed by evacuation of excess pyridine for 0.5 h. Then, the cell was heated to 423 K at a rate of 10 K min<sup>-1</sup> and kept at this temperature for 1.0 h to remove physisorbed pyridine. The concentration of the Brønsted and Lewis acid sites was calculated via Eqs. (1) and (2) respectively [44].

$$C_B (\mu\text{mol g}^{-1}) = \frac{1.88 \times IA_B \times R^2}{W} \quad (1)$$

$$C_L (\mu\text{mol g}^{-1}) = \frac{1.42 \times IA_L \times R^2}{W} \quad (2)$$

where  $C_B$  and  $C_L$  stand for the concentration of Brønsted and Lewis acid sites, respectively,  $IA_B$  and  $IA_L$  stand for the integrated absorbance peak at 1540 cm<sup>-1</sup> for Brønsted acid sites and peak at 1450 cm<sup>-1</sup> for Lewis acid sites, respectively,  $R$  stands for the radius of the self-supported disk and  $W$  stands for the weight of the sample.

#### 2.4. Catalytic activity test

Batch reactions were carried out in a Teflon-lined stainless steel autoclave (30 mL) with an external temperature controller. In a typical procedure, a mixture of butyl levulinate (BL, 2.0 mmol), catalyst (100 mg) and isopropanol (10 mL) were added to the Teflon liner. The reactor was sealed, purged with N<sub>2</sub> three times and pressurized to 1.0 MPa with N<sub>2</sub>. Subsequently, the autoclave was placed into a preheated oil-bath at the desired temperature and stirred at 800 rpm. When the designated time elapsed, the autoclave was cooled to ambient temperature with flowing water. After centrifugation (10000 rpm, 10 min) and filtration, the isolated solid catalyst was thoroughly washed using isopropanol (3 mL × 3) and dried at 333 K under vacuum for 4.0 h to test catalyst recyclability. The obtained solutions (including reaction and washing solutions) were mixed and diluted to 25 mL with isopropanol for qualitative and quantitative analysis. The regenerated catalyst was obtained by the calcination of the spent catalyst at 773 K for 4.0 h under air.

The catalyst leaching test was conducted under optimized conditions except for the reaction time. After the reaction time of 1.5 h, the autoclave was immediately cooled to room temperature using flowing water, then, the solid catalyst was removed, and the liquid phase was reheated to the desired temperature for a designated time.

#### 2.5. Product analysis

Qualitative product analysis was undertaken with gas chromatography-mass spectrometry (GC-MS, Agilent 7890B/5977A) based on an Agilent MS library. A HP-5 MS

capillary column (30 m × 250 μm × 0.25 μm) was used for product separation. The initial oven temperature was 323 K with a hold time of 1.0 min, then heated at a rate of 20 K min<sup>-1</sup> to 523 K where it was held for 1.0 min prior to cooling. Quantitative product analysis was performed on an Agilent GC-7890B gas chromatograph equipped with a flame ionization detector (FID) using the same capillary column and temperature program as those employed in GC-MS analysis with naphthalene as the internal standard. The BL conversion, GVL yield and selectivity were calculated according to Eqs. (3)–(5) respectively.

$$C_{BL} (\text{mol}\%) = \left( 1 - \frac{M_F}{M_I} \right) \times 100\% \quad (3)$$

$$Y_{GVL} (\text{mol}\%) = \frac{M_G}{M_I} \times 100\% \quad (4)$$

$$S_{GVL} (\text{mol}\%) = \frac{Y_{GVL}}{C_{BL}} \times 100\% \quad (5)$$

where  $C_{BL}$ ,  $Y_{GVL}$ ,  $S_{GVL}$ ,  $M_F$ ,  $M_I$  and  $M_G$  stand for the BL conversion, GVL yield, GVL selectivity, the final BL molar amount, the initial BL molar amount and the final GVL molar amount, respectively.

### 3. Result and discuss

#### 3.1. Catalyst characterization

FT-IR is used for functional group characterization of all samples (Fig. 1). Peaks at 3450 and 1630 cm<sup>-1</sup> are assigned to the stretching vibration of the –OH group on the catalyst surface and physically adsorbed water [45]. The band at 1069 cm<sup>-1</sup> is attributed to the stretching vibration of the P–O–Zr network [46]. The peak at 754 cm<sup>-1</sup> is ascribed to the deforming vibration of the P–O–P group [47], meanwhile, relative peak intensity of this group is observed to increase with P/Zr, indicating an increase in the amount of polyphosphate. The bands at 2350 and 528 cm<sup>-1</sup> are assigned to the stretching and deforming vibrations of the (P)–O–H group [48], respectively. As presented in Fig. 1, the aforementioned bands can be clearly observed in all samples, suggesting that as-synthesized catalysts are a mixture of phosphate, polyphosphate and hydrophosphates. XRD of the resulting catalysts indicate that they are amorphous in nature with no obvious diffraction lines relating to any crystalline zirconium phosphate phases (Fig. S1) [49,50].

The total acid sites of the catalysts were studied by NH<sub>3</sub>-TPD. Fig. 2 shows that all samples exhibit broad profiles in the range of 373–1073 K, indicating the coexistence of weak, moderate and strong acid sites (c.a. 447–454 K, 511–546 K and 671–744 K respectively) according to peak fitting deconvolution (Fig. S2). It shows clearly that the strength and sum of acid sites, by and large, increase

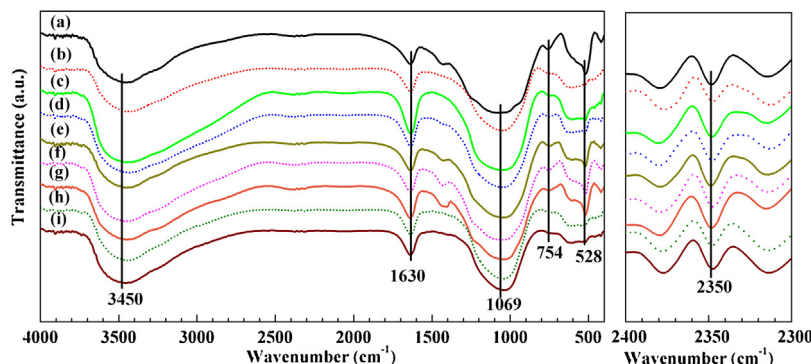


**Fig. 1.** FT-IR spectra of as-synthesized and used zirconium phosphate catalysts (a) ZrPO-0.50, (b) ZrPO-0.75, (c) ZrPO-1.00, (d) ZrPO-1.25, (e) ZrPO-1.50, (f) ZrPO-1.75, (g) ZrPO-2.00, (h) ZrPO-1.00 after the first cycle and (i) ZrPO-1.00 after the tenth cycle.

**Table 1**

Composition and acidic properties of as-synthesized, used and regenerated zirconium phosphate catalysts.

| Entry | Catalyst               | P/Zr <sup>a</sup> | S <sub>BET</sub> (m <sup>2</sup> g <sup>-1</sup> ) | Acid sites (μmol g <sup>-1</sup> ) |                       |                     |                    |                    |                       | X <sub>0.15</sub> |      |
|-------|------------------------|-------------------|--|------------------------------------|-----------------------|---------------------|--------------------|--------------------|-----------------------|-------------------|------|
|       |                        |                   |  | Weak <sup>b</sup>                  | Moderate <sup>b</sup> | Strong <sup>b</sup> | Total <sup>b</sup> | Lewis <sup>c</sup> | Brønsted <sup>c</sup> |                   |      |
| 1     | ZrPO-0.50              | 0.88              | 143.5  | —                                  | 77                    | 685                 | 762                | 153.5              | 28.8                  | 5.33              | 0.70 |
| 2     | ZrPO-0.75              | 1.12              | 185.0  | 262                                | 405                   | 643                 | 1310               | 177.5              | 37.2                  | 4.78              | 0.73 |
| 3     | ZrPO-1.00              | 1.33              | 248.5  | 384                                | 587                   | 919                 | 1890               | 187.8              | 40.0                  | 4.70              | 0.77 |
| 4     | ZrPO-1.25              | 1.56              | 253.0  | 415                                | 705                   | 1032                | 2152               | 173.9              | 49.1                  | 3.54              | 0.80 |
| 5     | ZrPO-1.50              | 1.92              | 275.5  | 493                                | 959                   | 1258                | 2710               | 174.0              | 71.8                  | 2.42              | 0.82 |
| 6     | ZrPO-1.75              | 2.14              | 275.0  | 513                                | 1131                  | 1254                | 2898               | 172.4              | 77.7                  | 2.22              | 0.84 |
| 7     | ZrPO-2.00              | 2.38              | 279.6  | 497                                | 1115                  | 963                 | 2575               | 174.2              | 113.8                 | 1.53              | 0.93 |
| 8     | ZrPO-1.00 <sup>d</sup> | 1.33              | 247.7  | 375                                | 569                   | 918                 | 1862               | 185.5              | 39.5                  | 4.69              | —    |
| 9     | ZrPO-1.00 <sup>e</sup> | 1.32              | 217.3  | 346                                | 534                   | 863                 | 1743               | 172.0              | 37.1                  | 4.63              | —    |
| 10    | ZrPO-1.00 <sup>f</sup> | 1.32              | 245.3  | 381                                | 575                   | 910                 | 1866               | 185.1              | 39.4                  | 4.69              | —    |

<sup>a,b,c</sup>Determined by ICP-AES, NH<sub>3</sub>-TPD, and Py-FTIR respectively.

<sup>d,e</sup>ZrPO-1.00 after the first and tenth cycle respectively.

<sup>f</sup>The regenerated ZrPO-1.00 catalyst after tenth cycle.

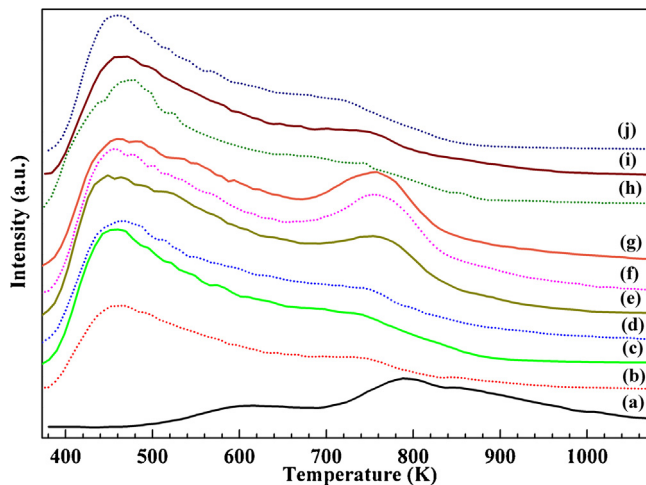


**Fig. 2.** NH<sub>3</sub>-TPD profiles of as-synthesized, used and regenerated zirconium phosphate catalysts (a) ZrPO-0.50, (b) ZrPO-0.75, (c) ZrPO-1.00, (d) ZrPO-1.25, (e) ZrPO-1.50, (f) ZrPO-1.75, (g) ZrPO-2.00, (h) ZrPO-1.00 after the first cycle, (i) ZrPO-1.00 after the tenth cycle and (j) the regenerated ZrPO-1.00 after the tenth.

with P/Zr. However, the strength of strong acid sites enhances significantly when P/Zr increases from 1.25 to 2.00, as indicated by the variation in maximized desorption temperatures from 672 to 744 K. This phenomenon can be attributed to increasing polyphosphate content, which can withdraw electrons from the residual phosphate groups on the surface [34]. The amount of different acid site strengths and total acid sites increase with P/Zr within the range 0.50–1.75, which can be attributed to the increase of surface area and phosphorus content [36,51]. However, further increasing P/Zr reduces the number of acid sites, this may be rationalized by the increase in polyphosphate content of ZrPO-2.00, which is consistent with the evident change in the P-O-P groups observed via FT-IR (Fig. 1 and Table 1).

To generate a concise understanding of the change in acidic species, the individual concentrations of Brønsted and Lewis acid sites on ZrPO-X samples are further quantified according to Py-FTIR (Fig. 3). The bands at 1450 and 1610 cm<sup>-1</sup> are attributed to pyridine adsorbed on Lewis acid sites, which include Zr—O—P and coordinatively unsaturated zirconium ions [36]. The vibrations at 1545 and 1640 cm<sup>-1</sup> are assigned to pyridine adsorbed on Brønsted acid sites of —P(OH)<sub>n</sub> (n = 1, 2) and the peak at 1490 cm<sup>-1</sup> is due to pyridine adsorbed on both Brønsted and Lewis acid sites [47]. As shown in Table 1, the Lewis acid concentrations of the catalysts possess a narrow range, from 153.5 to 187.8 μmol g<sup>-1</sup>, meaning that approximately constant accessible Lewis acid sites exists in all samples despite the reduced content of zirconium with increasing

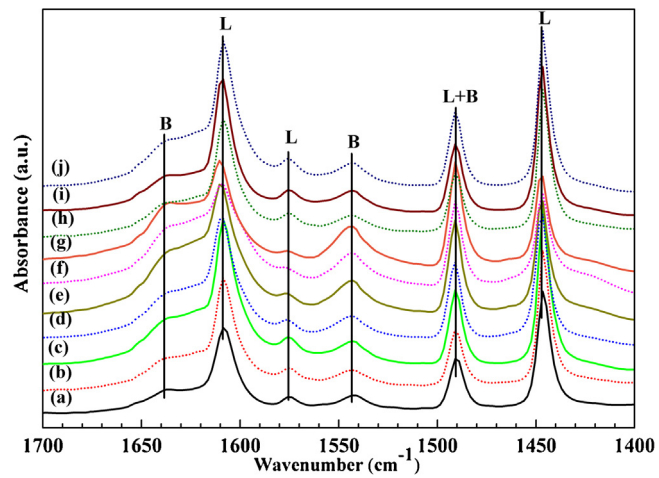


**Fig. 3.** FTIR spectra of pyridine absorbed at 423 K on as-synthesized, used and regenerated zirconium phosphate catalysts (a) ZrPO-0.50, (b) ZrPO-0.75, (c) ZrPO-1.00, (d) ZrPO-1.25, (e) ZrPO-1.50, (f) ZrPO-1.75, (g) ZrPO-2.00, (h) ZrPO-1.00 after the first cycle, (i) ZrPO-1.00 after the tenth cycle and (j) the regenerated ZrPO-1.00 after the tenth cycle.

P/Zr (confirmed by ICP-AES). Unlike Lewis acid sites, Brønsted acid site concentration sharply increases from 28.8 to 113.8 μmol g<sup>-1</sup> with P/Zr from 0.50 to 2.00, which can be attributed to the increase of phosphorus content, correspondingly, the molar ratio of Lewis to Brønsted acid concentration (L/B value) decreases markedly from 5.33 to 1.53. Therefore, we can conclude that the P/Zr ratio has a significant effect on Brønsted acid sites, while its influence on Lewis acid sites is negligible, i.e. the total acid concentration and L/B value can be readily tuned via the application of catalyst component modification.

The textural properties of various catalysts were characterized using N<sub>2</sub> physisorption. Results show that the surface area of the ZrPO-X catalyst increases with the P/Zr ratio between 0.50 and 1.50, little change is observed at 1.75 and a slight increase is found at 2.00 (Table 1). Compared with the surface area, the changes in pore volume and average pore diameter are different. They increase sharply when P/Zr increases from 0.50 to 1.25, and then both slightly decline with larger P/Zr values (Table S1). N<sub>2</sub> adsorption-desorption isotherms (Fig. S3) demonstrate that all catalysts exhibit typical type IV isotherms with H<sub>3</sub>-type hysteresis loops and a broad distribution of pore sizes. These indicate that the ZrPO-X materials have a layered structure, which is further confirmed by SEM images (Fig. S4). It has been reported that lower X<sub>0.15</sub> value indicates a more hydrophobic catalyst surface [41–43], the results listed in Table 1 clearly show that as the P/Zr ratio increases so does the X<sub>0.15</sub> value,

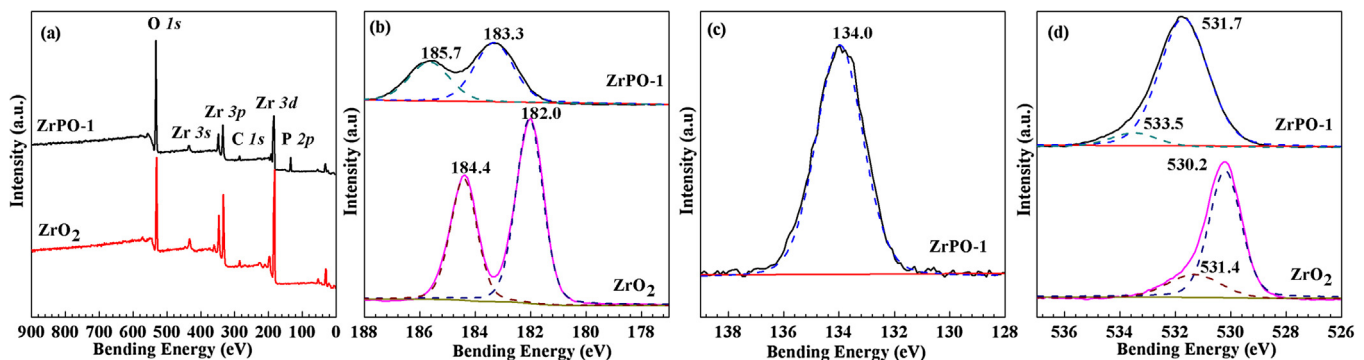


**Fig. 4.** XPS spectra of ZrPO-1.00 and ZrO<sub>2</sub> (a) survey scan, (b) high-resolution Zr 3d, (c) P 2p and (d) O 1s.

corresponding to an improvement in the hydrophilic character of the catalysts surface.

All samples possess similar XPS profiles (Fig. S6), peak-fitting deconvolution shows that all ZrPO-X materials exhibit significant increases in their Zr 3d and O 1s binding energies in comparison to that of ZrO<sub>2</sub> (Fig. 4, Table S2). This can be explained by the decrease of electron density of zirconium caused by the introduction of phosphorus [24] and the increase of surface hydroxyl groups [33] respectively. Zr 3d<sub>5/2</sub> and Zr 3d<sub>3/2</sub> binding energies increase from 182.0 and 184.4 eV (ZrO<sub>2</sub>) to 183.3 and 185.7 eV (ZrPO-1.00) respectively (Fig. 4b). Zr 3d and P 2p binding energies are found to increase with phosphorus content (Table S2). The former may be attributed to the increase in phosphorous content, which is known to effectively adjust the acidity of the zirconium Lewis acid sites [25,52,53], while the latter is associated with the formation of surface hydroxyl groups [34]. Similarly, the O 1s binding energies of the zirconium phosphate catalysts, in general, exhibit an increase trend with P/Zr, indicating the apparent change in the nature of oxygen. However, this general trend is not replicated for the deconvoluted components of O 1s signal (Table S2), which can be attributed to the diversity of oxygen-containing structures. For instance, O 1s of ZrPO-1.00 can be deconvoluted into two peaks situated at binding energies of 531.7 and 533.5 eV (Fig. 4d), which correspond to P—O—Zr (in coexistence with contributions from P=O, Zr—OH) [21] and P—O—H [54,55] respectively. XPS data listed in Table S2 indicates that surface P/Zr is similar to that of the bulk when it is in the range 0.50–1.25. However, this ratio is significantly lower than that of the bulk when more phosphorus is introduced. This suggests that polyphosphate is more likely to exist in the bulk phase, which results in a sharp increase in strong and total acid sites as discussed previously (Figs. 2, 3 and Table 1).

### 3.2. Catalytic activity evalution

#### 3.2.1. Catalyst screening

Catalytic performance of the prepared catalysts is investigated and the results are shown in Table 2. The degree of BL conversion is negligible in the absence of catalyst, indicating that BL is highly stable under non-catalyzed reaction conditions (Table 2, entry 1). However, in the presence of a ZrPO-X catalyst, the BL conversion and GVL yield increase substantially (Table 2, entries 2–8). 98.1% BL conversion and 95.7% GVL yield are obtained with ZrPO-1.00, both of which are similar to those of traditional Zr-containing materials, for example, ZrO<sub>2</sub> and Zr(OH)<sub>4</sub> (Table 2, entries 4, 11–12). Table 2 demonstrates that GVL is the dominant product as its selectivity is higher than 53.8% in each test, implying that efficient transfer hydrogenation of BL occurs over all ZrPO-X catalysts. Besides, trace amounts of isopropyl levulinate (*i*-PL) and its derivatives, isopropyl pent-2-enoate (*i*-PP2E), isopropyl pent-4-enoate (*i*-PP4E) and isopropyl 4-isopropoxypentanoate (*i*-P4(*i*-P)PA), are

also detected (the chemical structures of these compounds can be found in Table S3), suggesting the existence of intensive competition between transfer hydrogenation and *trans*-esterification during BL conversion.

It has been reported that Lewis acid sites are responsible for transfer hydrogenation of BL to butyl 2-hydroxypentanoate [22,30], which is further converted to GVL in the presence of Brønsted acid sites [32,33]. Therefore, a catalyst containing a suitable amount of both Lewis and Brønsted acid sites should favor BL transfer hydrogenation for this cascade process. For example, 98.1% BL conversion with 97.6% GVL selectivity are obtained when L/B is 4.70 (Table 2, entry 4). However, it is clear that excessive Brønsted acid sites lead to decreased BL conversion and GVL selectivity. For instance, when the L/B ratio decreases from 4.70 to 1.53, the BL conversion and GVL selectivity decrease from 98.1 and 97.6% to 32.5 and 53.8% respectively (Table 2, entries 4–8). This was further demonstrated upon addition of H<sub>3</sub>PO<sub>4</sub> to the reaction mixture which exhibited decreased GVL selectivity (Table 2, entry 9). This observation is in agreement with previous work undertaken with Zr-Beta, where, addition of H<sub>2</sub>SO<sub>4</sub> to the reaction mixture led to a significant decline in GVL yield [23]. The decreased trend of BL may be attributed to the decreased average pore size (Table S1) and the increased hydrophilicity of catalyst (Table 1). On the other hand, the lack of Brønsted acid sites results in inefficient BL transfer hydrogenation and a decline in potential GVL selectivity (the sum of GVL and *i*-PL). Simultaneously, by-products shift from *i*-PL to *i*-PP2E, *i*-PP4E and *i*-P4(*i*-P)PA, which indicates that limitation exists in the transformation of isopropyl 2-hydroxypentanoate to GVL (Table 2, entries 2–6). Hence, the introduction of phosphorus play a number of important roles: (a) increasing Lewis acid strengths which facilitates the step of MPV reduction of LA and its esters, (b) supplying suitable amount of Brønsted acid sites which benefits for the cyclization of the alkyl 2-hydroxypentanoate, (c) altering the textural properties and hydrophilicity of catalyst. Thus, it is important to keep a balance between Lewis and Brønsted acid sites to obtain high yield and selectivity of GVL, which explains the highest catalytic activity of ZrPO-1.00.

#### 3.2.2. Effect of catalyst dosage

Fig. 5 demonstrates that catalyst dosage is critical for BL transfer hydrogenation, where more ZrPO-1.00 results in improved BL conversion and GVL yield. The conversion of BL and the yield of GVL sharply increase from 78.4 and 58.7% to 98.1 and 97.6% respectively when the ZrPO-1.00 dosage increases from 50 to 100 mg. After which, changes in BL conversion and GVL yield are insignificant with a catalyst dosage of 125 mg, which indicates 100 mg of the catalyst would be the optimum amount under the reaction conditions.

**Table 2**

Catalytic activities of as-synthesized zirconium phosphate and other zirconium containing catalysts for transfer hydrogenation of BL.<sup>a</sup>

| Entry | Catalyst                                       | L/B  | Conv. (%)  | Yield (%)  |             |             |             |             | Sel. (%)   |
|-------|--|------|------------|------------|-------------|-------------|-------------|-------------|------------|
|       |  |      |            | GVL        | i-PL        | i-PP2E      | i-PP4E      | i-P4(i-P)PA |            |
| 1     | Blank  | –    | 1.2 ± 0.3  | ND         | 1.2 ± 0.3   | ND          | ND          | ND          | 0          |
| 2     | ZrPO-0.50                                      | 5.33 | 94.5 ± 2.0 | 85.3 ± 1.4 | 1.2 ± 0.79  | 1.3 ± 0.31  | 2.3 ± 1.10  | 4.4 ± 1.81  | 90.3 ± 1.7 |
| 3     | ZrPO-0.75                                      | 4.78 | 97.4 ± 1.1 | 90.7 ± 0.8 | 0.21 ± 0.19 | 1.47 ± 0.33 | 2.21 ± 0.21 | 2.81 ± 0.11 | 93.1 ± 2.3 |
| 4     | ZrPO-1.00                                      | 4.70 | 98.1 ± 1.8 | 95.7 ± 2.7 | 0.41 ± 0.32 | 0.53 ± 0.27 | 1.09 ± 0.23 | 0.37 ± 0.32 | 97.6 ± 1.4 |
| 5     | ZrPO-1.25                                      | 3.54 | 96.4 ± 2.3 | 83.7 ± 3.3 | 12.3 ± 2.3  | 0.11 ± 0.11 | 0.17 ± 0.09 | 0.13 ± 0.09 | 86.8 ± 3.1 |
| 6     | ZrPO-1.50                                      | 2.42 | 87.8 ± 1.5 | 66.8 ± 3.1 | 21.0 ± 4.1  | ND          | ND          | ND          | 76.2 ± 2.8 |
| 7     | ZrPO-1.75                                      | 2.22 | 65.4 ± 4.4 | 42.7 ± 4.9 | 22.7 ± 3.3  | ND          | ND          | ND          | 65.3 ± 3.3 |
| 8     | ZrPO-2.00                                      | 1.53 | 32.5 ± 3.7 | 17.5 ± 2.4 | 15.0 ± 3.2  | ND          | ND          | ND          | 53.8 ± 4.5 |
| 9     | ZrPO-1.00 <sup>b</sup>                         | 0.06 | 93.0 ± 3.4 | 64.0 ± 3.2 | 29.0 ± 4.3  | ND          | ND          | ND          | 68.8 ± 2.3 |
| 10    | NH <sub>4</sub> H <sub>2</sub> PO <sub>4</sub> | –    | 92.8 ± 1.7 | ND         | 92.8 ± 1.7  | ND          | ND          | ND          | 0          |
| 11    | Zr(OH) <sub>4</sub>                            | –    | 98.3 ± 1.1 | 92.4 ± 2.1 | 4.9 ± 1.3   | ND          | ND          | 1.0 ± 0.21  | 94.0 ± 3.1 |
| 12    | ZrO <sub>2</sub>                               | –    | 88.9 ± 2.7 | 79.5 ± 1.5 | 7.4 ± 2.4   | ND          | ND          | 2.0 ± 1.1   | 89.4 ± 1.8 |

<sup>a</sup> Reaction conditions: 2.0 mmol BL, 100 mg catalyst, 10 mL isopropanol, 483 K, 2.0 h, 1.0 MPa N<sub>2</sub>.

<sup>b</sup> adding 0.1 mmol H<sub>3</sub>PO<sub>4</sub>. ND: no detected.

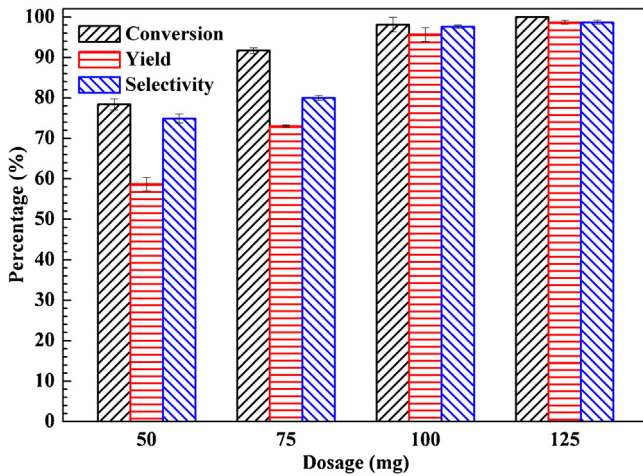


**Fig. 5.** Effect of ZrPO-1.00 dosage on transfer hydrogenation of BL to GVL. Reaction conditions: 2.0 mmol BL, 10 mL isopropanol, 483 K, 2.0 h, 1.0 MPa N<sub>2</sub>.

### 3.2.3. Effects of reaction temperature and time

**Fig. 6** illustrates the effects of reaction temperature and time on BL transfer hydrogenation. BL conversion substantially increases from 26.5 to 78.2% with a complimentary increase in GVL yield from 17.8 to 63.9% when the temperature increases from 453 to 483 K at 1.0 h. In contrast to the optimized conditions, a GVL yield

of 68.2% at a BL conversion of 78.2% is obtained at 453 K after 5.0 h, indicating the positive influence of temperature on BL conversion and GVL yield within the range explored. The major by-product *i*-PL exhibits a relatively minor increase with reaction time at 453 K, suggesting that lower temperatures may not be conducive towards the conversion of *i*-PL. At higher temperatures (463 and 473 K) an initial increase is found in the yield, but, at longer time on stream a gradual decline is observed. Similarly, an obvious increase in GVL (Fig. 6a) and the sum of other minor products (*i*-PP2E, *i*-PP4E or *i*-P4(*i*-P)PA, Fig. 6b) is found, indicating a favorable reaction route for the conversion of *i*-PL. At 483 K this effect is more pronounced at shorter time on stream, indicating that higher temperatures allow for more rapid conversion and a propensity towards increased initial formation of *i*-PL. However, this effect may simply be conversion based, specifically, when the achieved conversion increases beyond 90% the *i*-PL yield exhibits a decline, correlating with the formation of more GVL and additional products. The latter of which did not individually exhibit any correlation with time or temperature (Fig. S7). Regardless, it can be determined that increases in both time and temperature are beneficial for the formation of GVL.

### 3.2.4. Effects of various hydrogen donors

**Table 3** demonstrates that BL transfer hydrogenation is significantly influenced by the choice of the hydrogen-donating solvent. For example, little GVL is obtained when a primary alcohol (methanol or ethanol) is employed as the hydrogen donor,

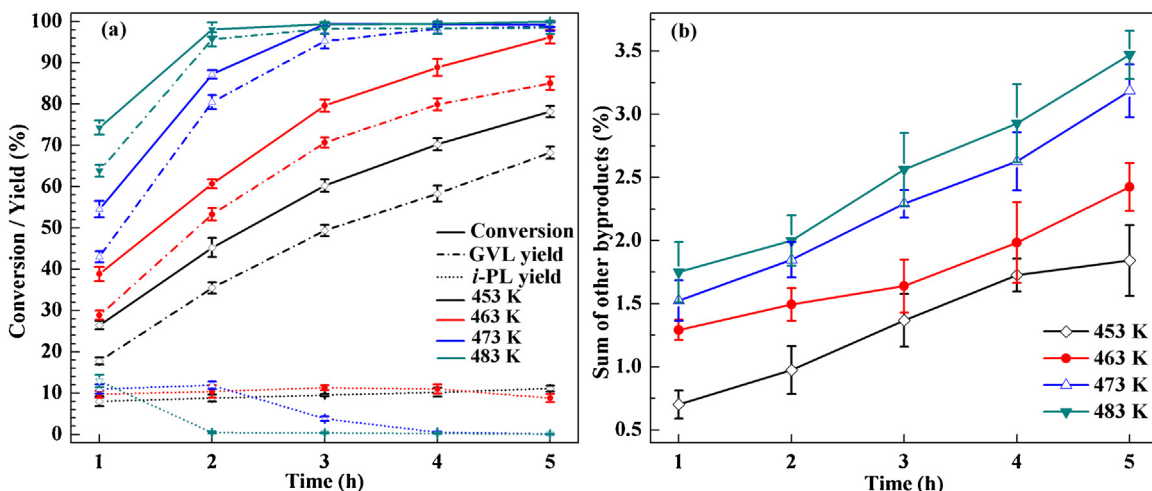


**Fig. 6.** Effect of reaction temperature and time on BL conversion and product distribution: (a) BL conversion, GVL and *i*-PL yield (b) sum of other byproducts. Reaction conditions: 2.0 mmol BL, 100 mg ZrPO-1.00, 10 mL isopropanol, 1.0 MPa N<sub>2</sub>.

**Table 3**The effect of hydrogen donor on BL transfer hydrogenation.<sup>a</sup>

| Entry | Hydrogen donor | Conv. (%)  | Yield (%) <sup>b</sup> |             |             |             | Sel. (%)    |
|-------|----------------|------------|------------------------|-------------|-------------|-------------|-------------|
|       |                |            |                        | GVL         | Ester       | Al-P2E      |             |
| 1     | Methanol       | 98.6 ± 0.3 | 0.6 ± 0.2              | 98.0 ± 1.2  | ND          | ND          | ND          |
| 2     | Ethanol        | 97.6 ± 1.2 | 11.1 ± 1.5             | 86.5 ± 3.8  | ND          | ND          | 11.4 ± 2.7  |
| 3     | Isopropanol    | 98.1 ± 1.8 | 95.7 ± 2.7             | 0.41 ± 0.32 | 0.53 ± 0.27 | 1.09 ± 0.23 | 0.37 ± 0.32 |
| 4     | 2-Butanol      | 95.4 ± 3.4 | 89.7 ± 1.8             | 2.13 ± 0.69 | 0.38 ± 0.13 | 0.76 ± 0.21 | 2.43 ± 0.47 |
| 5     | 2-Pentanol     | 90.9 ± 4.9 | 82.3 ± 2.3             | 3.17 ± 1.33 | 1.32 ± 1.06 | 1.68 ± 2.11 | 2.43 ± 0.59 |

<sup>a</sup> Reaction conditions: 2.0 mmol BL, 100 mg ZrPO-1.00, 10 mL solvent, 483 K, 2.0 h, 1.0 MPa N<sub>2</sub>.<sup>b</sup> Ester: alkyl levulinate; Al-P2E: alkyl pent-2-enoate; Al-P4E: alkyl pent-4-enoate; Al-4(Al)PA: alkyl 4-alkyloxypentanoate.

whereas levulinate ester, derived from BL *trans*-esterification, is found to be the dominant product (99.4% selectivity in methanol and 88.5% in ethanol, **Table 3**, entries 1 and 2 respectively). It is interesting to see that transfer hydrogenation performance is enhanced when a secondary alcohol is utilized, as indicated by the change in the product distribution. For example, 90.9% BL conversion with 90.5% GVL selectivity is achieved when 2-pentanol is used as the hydrogen donor, although trace amounts of 2-pentyl levulinate, 2-pentyl pent-2-enoate, 2-pentyl pent-4-enoate and 2-pentyl 2-pentyloxypentanoate are also generated (**Table 3**, Entry 5). According to van der Waal et al. [56], the reduction potential of the alcohol increases as follows: 2-pentanol < 2-butanol < isopropanol < ethanol < methanol (listed in Table S4), this indicates that primary alcohols have higher reduction potentials than secondary alcohols. Namely, secondary alcohols have stronger hydrogen donating capability than primary alcohols, which helps to explain the variation in BL transfer hydrogenation performance in the presence of different solvents.

As listed in Table S4, secondary alcohols show similar reduction potentials, however, it is of interest to note that the highest catalytic activity is obtained in isopropanol (**Table 3**, entry 3). This phenomenon may be explained by the steric effect of the solvent and the hydrophilicity of the catalyst. The former of which increases significantly with the elongation of the carbon chain, which results in reduced GVL production and modification of the product distribution. Previous studies demonstrate that the hydrophobicity of the catalyst has a positive influence on the transfer hydrogenation of the carbonyl group [23,56]. Here, the hydrophobicity of the alcohol is significantly enhanced with the elongation of the carbon chain. However, ZrPO-1.00 generally exhibits hydrophilic character due to the presence of P-OH groups. Therefore, suppression of the formed transition state between the catalyst and hydrogen donor is more pronounced in alcohols with longer carbon chains, which leads to reduced transfer hydrogenation activity even though lower reduction potential is displayed.

### 3.2.5. Effects of various substrates

Transfer hydrogenation of levulinate esters and LA were further investigated at 443 K up to 2.0 h. As listed in **Table 4** and presented in Fig. S8, the process efficiency exhibits significant differences according to the feedstock choice. Compared with levulinate esters, LA shows the best performance, 99.8% of LA conversion with 96.9% GVL yield can be obtained (**Table 4**, entry 1), this observation accords well with the work of Han et al. [25]. **Table 4** shows that the hydrophobicity and steric hindrance of the levulinate ester have significant influences on GVL production. It is well known that hydrophobicity of the substrate becomes more obvious with the elongation of the carbon chain of the alkyl group. In this study, methyl levulinate with less hydrophobic character is found to be the most active feedstock, giving 99.4% ML conversion and 62.8% GVL yield, while for the more hydrophobic butyl levulinate (BL), merely 35.8% BL conversion and 18.8% GVL yield can be obtained at the same reaction conditions (**Table 4**, entries 2 and 6). It should be

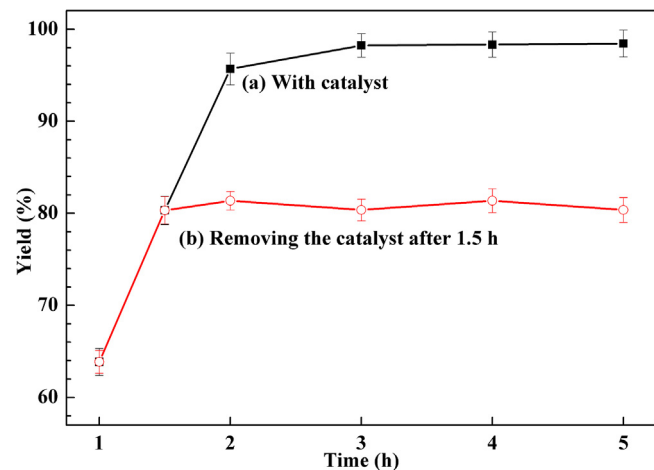


**Fig. 7.** Leaching test of ZrPO-1.00 for the transfer hydrogenation of BL to GVL. Reaction conditions: 2.0 mmol BL, 100 mg ZrPO-1.00, 10 mL isopropanol, 483 K, 1.0 MPa N<sub>2</sub>.

noted that *i*-PL shows poorer transfer hydrogenation performance than propyl levulinate due to steric hindrance (**Table 4**, entries 4–5). Besides, the ultimate selectivity of GVL is approximately 89.2% for *i*-PL as the substrate (Fig. S8), indicating that *i*-PL should maintain a moderate concentration in the conversion of LA and its ester to GVL.

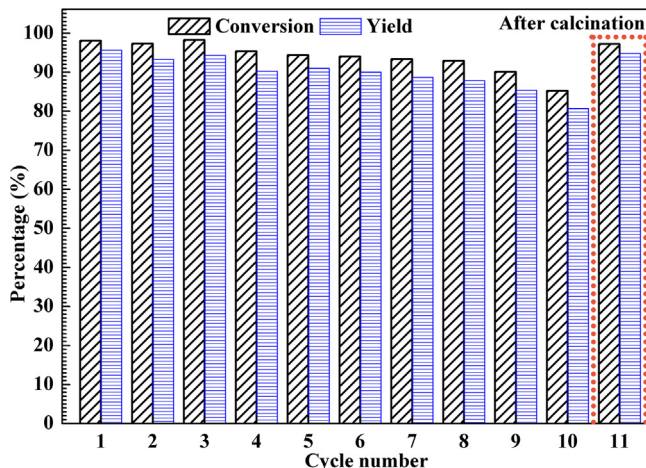
### 3.2.6. Catalyst leaching and reusability

Stability and reusability are crucial for an industrial catalyst, hence a leaching test under optimal conditions was undertaken. As displayed in **Fig. 7**, upon removing the catalyst at 1.5 h, the GVL yield remains at the same level, suggesting that no catalytically active phase is present. ICP-AES analysis shows that the concentrations of Zr<sup>4+</sup> and P<sup>5+</sup> in the filtrate are less than 1.0 ppm, thus, it is considered that catalyst leaching is negligible for this system. Examination of the reusability of ZrPO-1.00 demonstrates that this catalyst still maintains a relatively satisfactory activity after ten cycles (85.2% BL conversion and 80.7% GVL yield, **Fig. 8**), which confirms that this catalyst has reasonable stability.

However, there is a slight loss in catalytic activity after the tenth cycle as shown in **Fig. 8**, therefore, the fresh and used ZrPO-1.00 catalysts (after the first and tenth cycles) were comparatively characterized. Textural information obtained by N<sub>2</sub> adsorption-desorption isotherms demonstrates that the catalyst recovered after the first cycle and ZrPO-1.00 have similar surface areas and pore volumes, with only a small decrease of the average pore diameter (Fig. S10 and Table S1). But, these parameters are observed to decrease markedly after the tenth cycle, further analysis using ICP-AES (**Table 1**) and FT-IR spectra (**Fig. 1**) show that no obvious difference in absorbance occurs after the first and tenth cycles. This implies that the main component and characteristic functional groups of ZrPO-1.00 remain largely unchanged after transfer hydro-

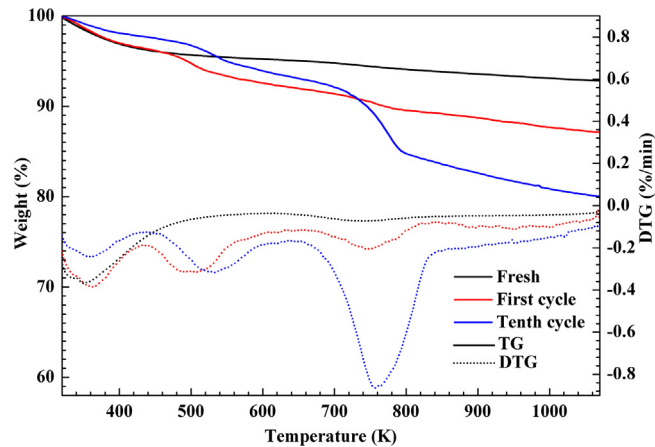
**Table 4**Effect of substrate on the transfer hydrogenation reaction.<sup>a</sup>

| Entry | Substrate <sup>b</sup> | Conv. (%)  | Yield (%)  | Sel. (%)   |             |             |             |            |
|-------|------------------------|------------|------------|------------|-------------|-------------|-------------|------------|
|       |                        |            |            | GVL        | i-PL        | i-PP2E      | i-PP4E      |            |
| 1     | LA                     | 99.8 ± 0.1 | 96.9 ± 2.8 | 2.9 ± 1.2  | ND          | ND          | ND          | 96.8 ± 2.4 |
| 2     | ML                     | 99.4 ± 0.3 | 62.8 ± 1.7 | 36.6 ± 2.8 | ND          | ND          | ND          | 63.2 ± 1.5 |
| 3     | EL                     | 85.4 ± 1.7 | 48.5 ± 2.2 | 32.5 ± 1.2 | 1.91 ± 0.18 | 1.58 ± 0.11 | 0.91 ± 0.24 | 56.8 ± 2.3 |
| 4     | PL                     | 60.4 ± 2.9 | 33.5 ± 1.8 | 22.9 ± 1.7 | 0.56 ± 0.09 | 1.86 ± 0.31 | 1.58 ± 0.07 | 55.5 ± 1.9 |
| 5     | i-PL                   | 10.9 ± 2.3 | 9.8 ± 3.8  | 89.1 ± 3.3 | 0.56 ± 0.21 | 0.34 ± 0.09 | 0.20 ± 0.11 | 89.9 ± 2.7 |
| 6     | BL                     | 35.8 ± 1.1 | 18.8 ± 1.5 | 13.3 ± 1.3 | 1.41 ± 0.17 | 1.13 ± 0.21 | 1.16 ± 0.32 | 52.5 ± 1.9 |

<sup>a</sup> Reaction conditions: 2.0 mmol substrate, 100 mg ZrPO-1.00, 10 mL isopropanol, 483 K, 2.0 h, 1.0 MPa N<sub>2</sub>.<sup>b</sup> ML, EL and PL stand for methyl levulinic acid, ethyl levulinic acid and propyl levulinic acid, respectively.**Fig. 8.** Catalyst recycle and regeneration of ZrPO-1.00 for the transfer hydrogenation of BL to GVL. Reaction conditions: 2.0 mmol BL, 100 mg ZrPO-1.00, 10 mL isopropanol, 483 K, 2.0 h, 1.0 MPa N<sub>2</sub>.

genation. XPS spectra (Fig. S11) reveal that the binding energies of Zr 3d, P 2p and O 1s show no change after the first cycle, but they shift to lower values after the tenth cycle, indicating that the chemical environment of ZrPO-1.00 gradually changes with increased cycle number. Meanwhile, a minor increase in the intensity of O 1s at 532.4 eV is found (Fig. S11), which may be assigned to the accumulation of active surface oxygen containing organic compounds.

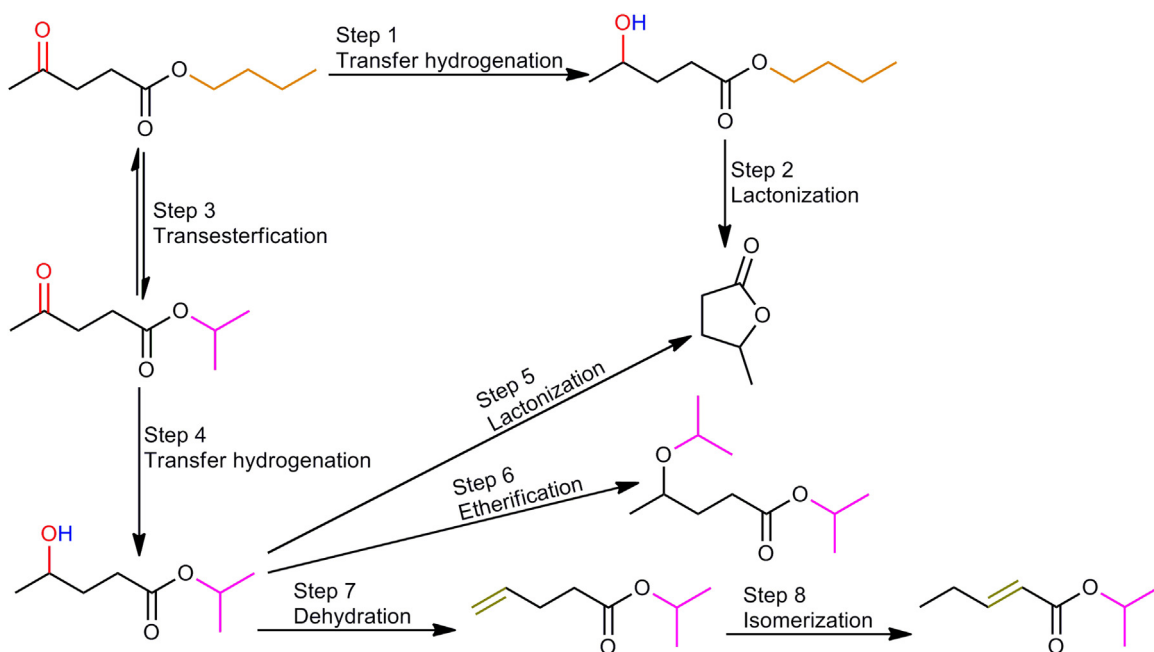
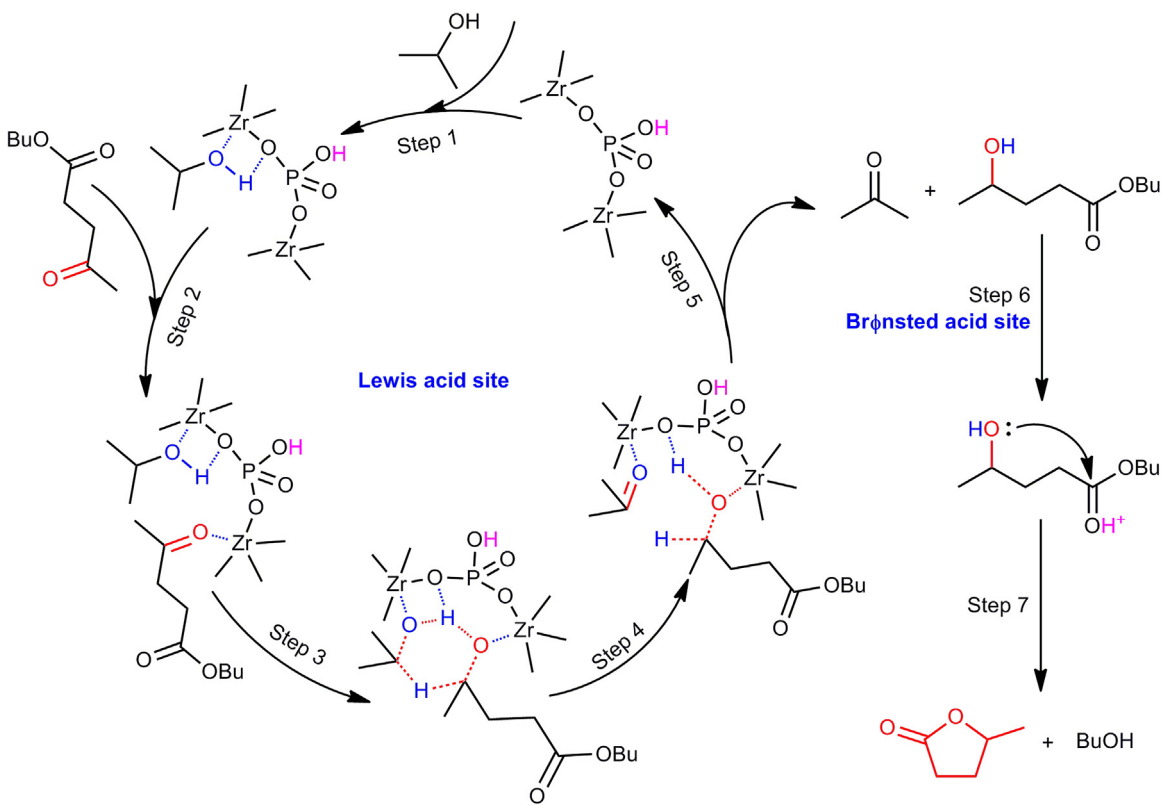
It is also observed that the color of the spent catalysts gradually change from white to pale yellow with increasing cycle number (Fig. S12). These observations were believed to be indicative of carbon deposition during the reaction, which was verified by elemental analysis, the carbon content was found to be 0.48 wt% after the first cycle and 5.78 wt% after the tenth cycle. This is also verified by TG/DTG analysis (Fig. 9). The curve of the fresh ZrPO-1.00 catalyst shows a continuous weight loss from 308 to 1073 K, this weight loss can be attributed to the volatilization of absorbed water (4.3 wt%, less than 473 K) and dehydroxylation of hydrophosphates in conjunction with the formation of pyrophosphates (3.1 wt%, above 473 K) [57]. But, the spent ZrPO-1.00 catalysts show different weight loss behaviors, where three weight loss regions are observed. The weight loss at temperature lower than 473 K can be attributed to the vaporization of physisorbed water and low boiling point reagents, while the weight loss above 473 K can be assigned to the vaporization/decomposition of chemisorbed reagents and/or high boiling point organic compounds on the catalysts surface. It is clear that the first weight loss remains constant after the first cycle and decreases to 2.8 wt% after the tenth cycle, indicating part of the moisture is replaced by absorbed organic chemicals, which vaporize and decompose at higher temperature. Fig. 9 demonstrates that the total weight loss is approximately 7.4 wt% for the fresh catalyst up to 1073 K, but this value increases to 12.9 and

**Fig. 9.** TG/DTG curves for the fresh and spent ZrPO-1.00 catalyst.

20.0 wt% for the spent catalysts after the first and tenth run, respectively. It was found that the catalyst after the tenth run could be effectively regenerated after calcination, exhibiting 97.2% BL conversion and 94.8% GVL yield (Fig. 8). As discussed above, this transfer hydrogenation process is promoted efficiently with zirconium phosphate possessing appropriate acid sites. Hence, the total acid amount and the L/B value fresh, spent and regenerated catalysts were compared (Table 1, entries 3 and 8–10). Results show that the changes of these values are negligible for the spent catalyst after the first run, whereas, both total acid site concentration and L/B ratio decrease from 1890 μmol g<sup>-1</sup>/4.70 to 1743 μmol g<sup>-1</sup>/4.63 for the fresh catalyst and the one after tenth cycle respectively, which can be completely recovered after calcination. In view of the results achieved from the TG-DTG and elemental analysis, this indicates clearly the Lewis acid sites are partly poisoned in preference to the Brønsted acid sites. Therefore, based on these results, it is suggested that organic species can accumulate on the Lewis acid sites gradually, this enrichment leads to a decline of the surface area, altered pore structure and a reduction in the L/B ratio, which are responsible for reduced catalytic activity during consecutive runs.

### 3.3. Reaction pathway and catalytic mechanism for BL transfer hydrogenation

Based on the qualitative identification of products via GC-MS (Table S3), insight obtained experimentally on the relationship between reaction parameters and product distribution, a probable reaction pathway for BL transfer hydrogenation can be proposed (Scheme 1). The carbonyl group of BL is first reduced to give an important intermediate, butyl 2-hydroxypentanoate, via transfer hydrogenation (Step 1), followed by lactonization of said intermediate yielding the desired product, GVL (Step 2). In addition, BL can also be converted to i-PL via trans-esterification with

**Scheme 1.** Reaction pathway of the transfer hydrogenation of BL to GVL over zirconium phosphate.**Scheme 2.** Catalytic mechanism for the transfer hydrogenation of BL to GVL over zirconium phosphate.

isopropanol (Step 3). After the same hydrogenation process as described above (BL hydrogenation), the obtained *i*-PL is hydrogenated to isopropyl 2-hydroxypentanoate (Step 4), which can be further converted to GVL (Step 5). Due to the existence of the active hydroxyl group in the molecule, isopropyl 2-hydroxypentanoate can be converted to isopropyl 2-isopropoxypentanoate by etheri-

fication with isopropanol (Step 6) [58–60]. Simultaneously, it can also be converted to isopropyl pent-4-enoate (Step 7) and its isomer isopropyl pent-2-enoate via catalytic dehydration (Step 8) [58]. It should be noted that two important intermediate products, butyl 4-hydroxypentanoate and isopropyl 4-hydroxypentanoate, were not detected by GC-MS, this can be attributed to their high activities

in the presence of Brønsted acid sites [31]. Therefore, it is suggested that the lactonization rate of intermediates is much faster than the levulinic esters hydrogenation rate. Namely, compared with lactonization, transfer hydrogenation is more likely to be the rate-determining step in this domino reaction pathway.

According to previous studies [24,25,61], the acid-base Zr(4<sup>+</sup>)-O(2<sup>-</sup>) pairs play an important role in the MPV reaction. However, the binding energies of Zr 3d and O 1s generally increase with increasing phosphorus content respectively (Fig. S5), the change of the former promotes the formation of the transition state but an inverse effect is shown for the change of the latter. Simultaneously, the catalytic activity increases when P/Zr enlarges from 0.50 to 1.00, indicating that the acid sites play a more important role than basic sites. In addition, a lower temperature is needed when LA is used as the feedstock, which is the opposite of that observed over amphoteric ZrO<sub>2</sub> [19], this finding further verifies the above observations regarding the role of acid sites. Therefore, Lewis acid sites dominate the MPV reduction, while the basic sites are auxiliary in ZrPO-X promoted reactions. Meanwhile, a suitable amount of Brønsted acid sites play a promotional role to enhance the conversion of alkyl 4-hydroxypentanoate to GVL. Based on this theory, a plausible catalytic mechanism for this efficient GVL production process is proposed. As displayed in Scheme 2, isopropanol is first absorbed on the active site of the catalyst, then the hydroxyl is coordinated and stabilized by Lewis acid sites and the oxo-ion site (step 1). Like many GVL formation processes over Zr-containing catalysts, the carbonyl of BL is subsequently activated by Lewis acid sites (step 2). A hydride shift between the hydrogen donor and the carbonyl of BL occurs via the formation of a cyclic six-membered transition state (step 3 and 4), giving acetone and butyl 4-hydroxypentanoate as the products (step 5). Finally, butyl 4-hydroxypentanoate is converted to GVL via Brønsted acid catalyzed intramolecular cyclization over ZrPO-1.00 (step 6 and 7).

## 4. Conclusions

The cost-effective ZrPO-X material is found to be an efficient and robust catalyst for GVL formation via levulinic ester transfer hydrogenation due to the synergistic effect of Brønsted and Lewis acid sites. Under optimized reaction conditions, 98.1% BL conversion can be obtained with a 95.7% GVL yield over ZrPO-1.00. Furthermore, GVL production is extremely sensitive to the L/B ratio which can be simply adjusted by the change of zirconium and phosphorous atom contents. Suitable quantities of Brønsted acid sites have a positive effect on the GVL yield. Finally, the optimized catalyst, ZrPO-1.00, is highly stable and can be reused for at least ten runs. Therefore, the presented catalytic system has great potential for GVL production from renewable lignocellulosic biomass due to its high efficiency, simple technology, and excellent catalyst reusability.

## Acknowledgements

This work was supported by the Natural Science Foundation of China (21336002, 21690083 and 21676108) and the Natural Science Foundation of Guangdong Province, China (2015A030311048).

## Appendix A. Supplementary data

Supplementary data associated with this article can be found, in the online version, at <http://dx.doi.org/10.1016/j.apcatb.2017.05.013>.

## References

- [1] J.N. Chheda, G.W. Huber, J.A. Dumesic, *Angew. Chem. Int. Ed.* 46 (2007) 7164–7183.
- [2] C.O. Tuck, E. Pérez, I.T. Horváth, R.A. Sheldon, M. Poliakoff, *Science* 337 (2012) 695–699.
- [3] P. Gallezot, *Chem. Soc. Rev.* 41 (2012) 1538–1558.
- [4] D.M. Alonso, S.G. Wettstein, J.A. Dumesic, *Green Chem.* 15 (2013) 584–595.
- [5] D. Rasina, A. Kahler-Quesada, S. Ziarelli, S. Warratz, H. Cao, S. Santoro, L. Ackermann, L. Vaccaro, *Green Chem.* 18 (2016) 5025–5030.
- [6] J.S. Luterbacher, J.M. Rand, D.M. Alonso, J. Han, J.T. Youngquist, C.T. Maravelias, B.F. Pfleger, J.A. Dumesic, *Science* 343 (2014) 277–280.
- [7] K. Yan, Y. Yang, J. Chai, Y. Lu, *Appl. Catal. B: Environ.* 179 (2015) 292–304.
- [8] F.D. Pileidis, M.-M. Titirici, *ChemSusChem* 9 (2016) 562–582.
- [9] H. Li, Z. Fang, J. Luo, S. Yang, *Appl. Catal. B: Environ.* 200 (2017) 182–191.
- [10] F. Liguori, C. Moreno-Marrodan, P. Barbaro, *ACS Catal.* 5 (2015) 1882–1894.
- [11] W. Luo, M. Sankar, A.M. Beale, Q. He, C.J. Kiely, P.C.A. Bruijnincx, B.M. Weckhuysen, *Nat. Commun.* 6 (2015) 6540–6549.
- [12] S. Cao, J.R. Monnier, C.T. Williams, W. Diao, J.R. Regalbuto, *J. Catal.* 326 (2015) 69–81.
- [13] D. Wang, D. Astruc, *Chem. Rev.* 115 (2015) 6621–6686.
- [14] M.J. Gilkey, B. Xu, *ACS Catal.* 6 (2016) 1420–1436.
- [15] P.J.C. Hausoul, C. Broicher, R. Vegliante, C. Göb, R. Palkovits, *Angew. Chem. Int. Ed.* 55 (2016) 5579–5601.
- [16] S. Zhu, Y. Xue, J. Guo, Y. Cen, J. Wang, W. Fan, *ACS Catal.* 6 (2016) 2035–2042.
- [17] Z. Yang, Y.-B. Huang, Q.-X. Guo, Y.-F. Yu, *Chem. Commun.* 49 (2013) 5328–5330.
- [18] R.R. Gowda, E.Y.X. Chen, *ChemSusChem* 9 (2016) 181–185.
- [19] X. Tang, Z. Li, X. Zeng, Y. Jiang, S. Liu, T. Lei, Y. Sun, L. Lin, *ChemSusChem* 8 (2015) 1601–1607.
- [20] M. Chia, J.A. Dumesic, *Chem. Commun.* 47 (2011) 12233–12235.
- [21] X. Tang, H. Chen, L. Hu, W. Hao, Y. Sun, X. Zeng, L. Lin, S. Liu, *Appl. Catal. B: Environ.* 147 (2014) 827–834.
- [22] J. Wang, S. Jaenicke, G.-K. Chuah, *RSC Adv.* 4 (2014) 13481–13489.
- [23] L. Bui, H. Luo, W.R. Gunther, Y. Román-Leshkov, *Angew. Chem. Int. Ed.* 52 (2013) 8022–8025.
- [24] J. Song, L. Wu, B. Zhou, H. Zhou, H. Fan, Y. Yang, Q. Meng, B. Han, *Green Chem.* 17 (2015) 1626–1632.
- [25] J. Song, B. Zhou, H. Zhou, L. Wu, Q. Meng, Z. Liu, B. Han, *Angew. Chem. Int. Ed.* 54 (2015) 9399–9403.
- [26] X. Tang, X. Zeng, Z. Li, W. Li, Y. Jiang, L. Hu, S. Liu, Y. Sun, L. Lin, *ChemCatChem* 7 (2015) 1372–1379.
- [27] Z. Xue, J. Jiang, G. Li, W. Zhao, J. Wang, T. Mu, *Catal. Sci. Technol.* 6 (2016) 5374–5379.
- [28] A.H. Valekar, K.-H. Cho, S.K. Chitale, D.-Y. Hong, G.-Y. Cha, U.H. Lee, D.W. Hwang, C. Serre, J.-S. Chang, Y.K. Hwang, *Green Chem.* 18 (2016) 4542–4552.
- [29] J. Zhang, J. Chen, Y. Guo, L. Chen, *ACS Sustain. Chem. Eng.* 3 (2015) 1708–1714.
- [30] J. He, H. Li, Y.-M. Lu, Y.-X. Liu, Z.-B. Wu, D.-Y. Hu, S. Yang, *Appl. Catal. A: Gen.* 510 (2016) 11–19.
- [31] H.Y. Luo, D.F. Consoli, W.R. Gunther, Y. Román-Leshkov, *J. Catal.* 320 (2014) 198–207.
- [32] O.A. Abdelrahman, A. Heyden, J.Q. Bond, *ACS Catal.* 4 (2014) 1171–1181.
- [33] Y. Kuwahara, H. Kango, H. Yamashita, *ACS Sustain. Chem. Eng.* 5 (2017) 1141–1152.
- [34] R. Weingarten, Y.T. Kim, G.A. Tompsett, A. Fernández, K.S. Han, E.W. Hagaman, W.C. Conner Jr., J.A. Dumesic, G.W. Huber, *J. Catal.* 304 (2013) 123–134.
- [35] J. Tuteja, H. Choudhary, S. Nishimura, K. Ebihani, *ChemSusChem* 7 (2013) 123–134.
- [36] V.V. Ordovsky, J. van der Schaaf, J.C. Schouten, T.A. Nijhuis, *ChemSusChem* 5 (2012) 1812–1819.
- [37] V.V. Ordovsky, V.L. Sushkevich, J.C. Schouten, J. van der Schaaf, T.A. Nijhuis, *J. Catal.* 300 (2013) 37–46.
- [38] R. Weingarten, G.A. Tompsett, W.C. Conner Jr., G.W. Huber, *J. Catal.* 279 (2011) 174–182.
- [39] G. Gliozzi, A. Innorta, A. Mancini, R. Bortolo, C. Perego, M. Ricci, F. Cavani, *Appl. Catal. B: Environ.* 145 (2014) 24–33.
- [40] O.A. Rusu, W.F. Hoelderich, H. Wyart, M. Ibert, *Appl. Catal. B: Environ.* 176–177 (2015) 139–149.
- [41] M. Thommes, S. Mitchell, J. Pérez-Ramírez, *J. Phys. Chem. C* 116 (2012) 18816–18823.
- [42] D. Song, S. An, Y. Sun, Y. Guo, *J. Catal.* 333 (2016) 184–199.
- [43] I. Ogino, Y. Suzuki, S.R. Mukai, *ACS Catal.* 5 (2015) 4951–4958.
- [44] N.A.S. Ramli, N.A.S. Amin, *Appl. Catal. B: Environ.* 163 (2015) 487–498.
- [45] X.-Z. Lin, T.-Z. Ren, Z.-Y. Yuan, *Catal. Sci. Technol.* 5 (2015) 1485–1494.
- [46] Z. Miao, L. Xu, H. Song, H. Zhao, L. Chou, *Catal. Sci. Technol.* 3 (2013) 1942–1954.
- [47] J. Jiménez-Jiménez, P. Maireles-Torres, P. Olivera-Pastor, E. Rodríguez-Castellón, A. Jiménez-López, D.J. Jones, J. Rozière, *Adv. Mater.* 10 (1998) 812–815.
- [48] Q.-Y. Liu, Y.-H. Liao, T.-J. Wang, C.-L. Cai, Q. Zhang, N. Tsubaki, L.-L. Ma, *Ind. Eng. Chem. Res.* 53 (2014) 12655–12664.
- [49] S. Komarneni, Q.H. Li, R. Roy, *J. Mater. Chem.* 4 (1994) 1903–1906.
- [50] P. Jiang, B. Pan, B. Pan, W. Zhang, Q. Zhang, *Colloid Surf. A* 322 (2008) 108–112.
- [51] S.K. Das, M.K. Bhunia, A.K. Sinha, A. Bhaumik, *ACS Catal.* 1 (2011) 493–501.
- [52] H.J.M. Bosman, A.P. Pijpers, A.W.M.A. Jaspers, *J. Catal.* 161 (1996) 551–559.
- [53] H. Li, Z. Fang, J. He, S. Yang, *ChemSusChem* 10 (2017) 681–686.

- [54] X.-Z. Lin, Z.-Y. Yuan, Eur. J. Inorg. Chem. 2012 (2012) 2661–2664.
- [55] B. Pawelec, S. Murcia-Mascarós, J.L.G. Fierro, Langmuir 18 (2002) 7953–7963.
- [56] J.C. van der Waal, P.J. Kunkeler, K. Tan, H. van Bekkum, J. Catal. 173 (1998) 74–83.
- [57] M. Zamin, T. Shaheen, A. Dyer, J. Radioanal. Nucl. Chem. 182 (1994) 323–333.
- [58] R. Palkovits, Angew. Chem. Int. Ed. 49 (2010) 4336–4338.
- [59] J.-P. Lange, J.Z. Vesterling, R.J. Haan, Chem. Commun. 33 (2007) 3488–3490.
- [60] X.-L. Du, Q.-Y. Bi, Y.-M. Liu, Y. Cao, K.-N. Fan, ChemSusChem 4 (2011) 1838–1843.
- [61] S.H. Liu, S. Jaenicke, G.K. Chuah, J. Catal. 206 (2002) 321–330.